INFLUENCE OF VARIOUS UNSTEADY AERODYNAMIC MODELS ON THE AEROMECHANICAL STABILITY OF A HELICOPTER IN GROUND RESONANCE*

P.P. Friedmann
Professor of Engineering and Applied Science

and

C. Venkatesan
Assistant Research Engineer
Mechanical, Aerospace and Nuclear Engineering Department
University of California, Los Angeles, California 90024

Abstract

The aeromechanical stability of a helicopter in ground resonance was analyzed, by incorporating five different aerodynamic models in the coupled rotor/fuselage analysis. The sensitivity of the results to changes in aerodynamic modelling was carefully examined. The theoretical results were compared with experimental data and useful conclusions are drawn regarding the role of aerodynamic modeling on this aeromechanical stability problem. The aerodynamic model which provided the best all around correlation with the experimental data was identified.

Nomenclature

a	- lift curve slope
C	- lift deficiency factor
C_1	- coefficient in inflow equations, C_1 = 0.5 or 1.0
C_T	- Thrust coefficient
C_{Mx}, C_{My}	- moment coefficients in roll and pitch
$[L]$	- induced flow matrix
$\dot{m}$	- mass flow rate
M	- rotor aerodynamic moment
M_1	- apparent inertia
r	- radial location of a typical blade section
R	- rotor radius
s	- eigenvalue
dT	- differential thrust
β_{1c}, β_{1s}	- cyclic flap coordinates
β_P, β_R	- progressing and regressing flap modes respectively
γ	- Lock number
γ^*	- equivalent, reduced or effective Lock number
λ_0	- steady or mean inflow
λ	- total inflow, $\lambda = \lambda_0 + \delta\lambda$; also inflow mode, in figures only
$\lambda_1, \lambda_{1c}, \lambda_{1s}$	- inflow variables
$\delta\lambda$	- unsteady wake induced perturbational inflow
ω	- modal frequency, imaginary part of s
Ω	- rotor R.P.M.
ϕ	- body roll mode
ψ	- azimuthal angle or nondimensional time $\psi = \Omega t$
ρ	- density of air
σ	- modal damping, real part of s
$\bar{\sigma}$	- solidity ratio
θ	- body pitch mode
θ_c	- collective pitch setting of the blade
ζ_{1c}, ζ_{1s}	- cyclic lag coordinates
ζ_P, ζ_R	- progressing and regressing lag modes respectively

1. Introduction

Unsteady aerodynamics have a significant influence on the aeroelastic and the aeromechanical stability characteristics of helicopters. The mathematical sophistication of refined unsteady aerodynamic models is sometimes prohibitive to incorporate in the aeroelastic analyses and therefore it is quite frequent that rotary-wing aeroelastic analyses are based upon quasisteady aerodynamic theory. Fortunately, there are some relatively simple unsteady aerodynamic models, known as inflow models, which can be conveniently incorporated in the aeroelastic and aeromechanical studies of helicopters. These simple models are based upon the definition of certain inflow parameters which represent essentially the unsteady wake-induced flow through the rotor disk. A number of such inflow models are available in the literature; however the applicability of a particular model to a given rotor dynamic problem and the sensitivity of the stability boundaries to the choice of the inflow model and comparisons with experimental data have not been considered in detail in the literature. Bousman[1] has carried out an experimental study of the aeromechanical stability of a hingeless rotor supported on a special gimbal which simulated the pitch and roll degrees of freedom. The availability of this high quality experimental data provides an

*This research was supported by NASA Grant NAG 2-209, funded by Ames Research Center, Moffett Field, California

opportunity; (a) to test the validity of mathematical models representing the coupled rotor/fuselage dynamics and (b) to determine the influence of various aerodynamic models on this aeromechanical problem. Bousman attributed some of the discrepancies, found between the theoretical results presented in his paper and the experimental results, to dynamic inflow. This conclusion was examined by Johnson[2], in a recent study, where the unsteady aerodynamic effects on the rotor were represented by a dynamic inflow model[3]. Johnson's[2] results with the dynamic inflow model[3,4] indicated better agreement with the experimental data than the results obtained using the quasi-steady aerodynamic model. Using the coupled rotor/body model[5,6] with simple quasi-steady aerodynamics, the authors[7] also obtained good agreement with the experimental results generated by Bousman[1]. Based on the agreement with the experimental data, they concluded that the coupled rotor/fuselage model developed, was reliable.

The purpose of this study is to extend Ref. 7 and study the sensitivity of the results obtained to changes in the aerodynamic assumptions used. To accomplish this objective, five different aerodynamic models were incorporated in the mathematical model representing the coupled rotor/fuselage dynamics and the sensitivity of the stability boundaries to changes in aerodynamic modelling was determined. The theoretical results were compared with the experimental data and based on this comparison, conclusions are drawn regarding the selection of the parameters used in defining these aerodynamic models.

2. Aerodynamic Models Used in the Analysis

The aerodynamic models, incorporated in this aeromechanical stability study representing a coupled rotor/fuselage system, were: (a) quasi-steady aerodynamics, (b) two different perturbation inflow models and (c) two different dynamic inflow models. A brief description of these aerodynamic models is provided below.

Quasi-steady Aerodynamic Model

The quasi-steady aerodynamic model, employed in the analysis, is based on Greenberg's[8] formulation of unsteady aerodynamic loads on an oscillatory airfoil in a pulsating flow. Greenberg's theory is a modified form of Theodorsen's unsteady aerodynamic theory. The quasi-steady model is obtained by assuming $C(k) = 1$ and neglecting the apparent mass terms (noncirculatory terms). In this model, the assumption of $C(k) = 1$ implies that the unsteady wake effects are totally neglected.

Inflow Models

The inflow models represent the unsteady wake effects in a simple form. In these models, the unsteady wake-induced flow through the rotor disk is defined by a set of inflow variables and these variables essentially provide a correction to the inflow assumed in the quasi-steady aerodynamic theory. When inflow models are used in the analysis of rotor dynamic problems the blade loads have to be calculated from the quasi-steady aerodynamic expressions. An important fact to be noted is that the quasi-steady aerodynamic model is a two dimensional local model and hence it is applied at a typical cross section located at a spanwise station along the rotor blade, in the blade fixed, rotating coordinate system. On the other hand, the inflow models represent the global effects of the unsteady wake and therefore they are applicable to the complete rotor. The various inflow models are described below.

Perturbation Inflow Model

Prior to describing the perturbation inflow model, it is useful to clarify certain aspects of the terminology used in the literature which deals with this subject. In some cases, the perturbation inflow model is referred to as quasi-static inflow model[2] and in other cases as quasi-steady inflow model[9].

The induced flow-field acting on a helicopter rotor affects both rotor equilibrium (trim loadings) and rotor response (transient loading). Therefore, it is reasonable to assume that the induced flow will also be affected by the oscillations of the rotor. This assumption is the basis of both the perturbation inflow models and dynamic inflow models. A detailed derivation of these inflow models can be found in Refs. 3 and 9.

In these models the total induced velocity on the rotor disk due to the wake is assumed to consist of two parts: (1) a steady inflow, λ_0, (for trim loadings) and (2) a perturbation inflow, $\delta\lambda$, (for transient loadings). Therefore, the total induced velocity normal to the rotor disk is expressed as

$$\lambda = \lambda_0 + \delta\lambda \tag{1}$$

Assuming that the perturbation inflow, $\delta\lambda$, varies azimuthally as well as linearly along the radius, the total inflow can be written as

$$\lambda = \lambda_0 + \lambda_1 + \lambda_{1c}\frac{r}{R}\cos\psi + \lambda_{1s}\frac{r}{R}\sin\psi \tag{2}$$

where the inflow variables λ_1, λ_{1c}, λ_{1s} are functions of time. These inflow variables are related to the perturbational thrust, roll and pitch moment coefficients through the following relation.

$$[L]^{-1}\begin{Bmatrix}\lambda_1\\ \lambda_{1c}\\ \lambda_{1s}\end{Bmatrix} = \begin{Bmatrix}C_T\\ -C_{My}\\ C_{Mx}\end{Bmatrix}_{P.A} \tag{3}$$

where P.A stands for perturbational aerodynamics. The elements of [L] can be obtained either theoretically, by using momentum theory[3,9] or experimentally[10].

In ground resonance type of aeromechanical problems, the inflow variable λ_1 does not couple with the body and cyclic blade degrees of freedom and hence it does not have to be considered in the analysis. Thus only the equations for the inflow variables λ_{1c} and λ_{1s} are relevant to this specific problem and these can be written as

$$[L]^{-1}\begin{Bmatrix}\lambda_{1c}\\ \lambda_{1s}\end{Bmatrix} = \begin{Bmatrix}-C_{My}\\ C_{Mx}\end{Bmatrix}_{P.A} \tag{4}$$

For axial flow through the rotor, which corresponds to the present case, the elements of [L] can be obtained by applying momentum theory[9]. The differential thrust on an elemental area dA (= rdrdψ) of the disk is related to the inflow by the equation

$$dT = \dot{m}\, 2\lambda\Omega R \tag{5}$$

It should be mentioned that by relating the total differential thrust (steady and perturbation) to the total induced velocity (steady and perturbation) in the form, given in Eq. (5), it is assumed that the thrust-inflow relation is the same for steady as well as perturbational conditions. This basic assumption implies that the variation of the forces on the rotor is sufficiently slow so that the classical actuator disk theory is valid for both steady and perturbational inflow velocities. Therefore, this inflow theory is also recognized to be a low frequency approximation to the unsteady aerodynamics of the rotor.

Following Johnson[2], the mass flow rate in Eq. (5) can be written as

$$\dot{m} = \rho\lambda_0\Omega R dA \tag{6}$$

It is important to note that the mass flow rate is defined with respect to the steady or mean value of the inflow λ_0.

The aerodynamic pitch and roll moments on the rotor disk, acting at the hub, can be obtained by taking moments of the elemental thrust about the hub center and integrating over the complete rotor disk. The pitch and roll moments are

$$M_{pitch} = \int_0^R \int_0^{2\pi} -r\cos\psi dT \tag{7}$$

$$M_{roll} = \int_0^R \int_0^{2\pi} r\sin\psi dT \tag{8}$$

Substituting Eqs. (2), (5) and (6) in Eqs. (7) and (8) and integrating, the pitch and roll moments become

$$-M_{pitch} = \frac{\pi}{2}\rho R^3\lambda_0\lambda_{1c}(\Omega R)^2 \tag{9}$$

$$M_{roll} = \frac{\pi}{2}\rho R^3\lambda_0\lambda_{1s}(\Omega R)^2 \tag{10}$$

After nondimensionalization, the relation between inflow variables and the perturbational aerodynamic moment coefficients becomes

$$\begin{bmatrix} \frac{\lambda_0}{2} & 0 \\ 0 & \frac{\lambda_0}{2} \end{bmatrix} \begin{Bmatrix} \lambda_{1c} \\ \lambda_{1s} \end{Bmatrix} = \begin{Bmatrix} -C_{My} \\ C_{Mx} \end{Bmatrix}_{P.A} \tag{11}$$

On the other hand, if the mass flow rate $\dot{m}$, is defined as (following Peters and Gaonkar[9])

$$\dot{m} = \rho\lambda\Omega R dA \tag{12}$$

where the mass flow is defined with respect to the total induced velocity λ, the inflow equations for λ_{1c} and λ_{1s} become

$$\begin{bmatrix} \lambda_0 & 0 \\ 0 & \lambda_0 \end{bmatrix} \begin{Bmatrix} \lambda_{1c} \\ \lambda_{1s} \end{Bmatrix} = \begin{Bmatrix} -C_{My} \\ C_{Mx} \end{Bmatrix}_{P.A} \tag{13}$$

Comparing Eqs. (11) and (13), it is evident that depending on the definition of mass flow rate, i.e. Eq. (6) or (12), the coefficients of the elements of $[L]^{-1}$ matrix differ by a factor of two.

Equations (11) or (13) are complete only after identifying the right hand side. This is done by obtaining expressions for the moment coefficients using blade element theory. Once these have been obtained, a relation is established between the inflow variables and rotor blade motion. It was shown in Refs. 3, 9 and 11 that incorporation of a perturbational inflow model, as represented by Eq. (11) or (13), in rotor dynamic problems yields a modification of the aerodynamic loads acting on the blade which can be represented by a reduced or effective Lock number

$$\gamma^* = C\gamma \tag{14}$$

If Eq. (11) is used in the rotor dynamic problem, the lift deficiency factor C becomes

$$C = \frac{1}{1 + \frac{\bar{\sigma}a}{8\lambda_0}} \tag{15}$$

This factor is found to be equal to the low frequency approximation of Loewy's lift deficiency function for harmonic loadings[3]. On the other hand, Eq. (13) produces a lift deficiency factor

$$C = \frac{1}{1 + \frac{\bar{\sigma}a}{16\lambda_0}} \tag{16}$$

which is higher than that given in Eq. (15).

The two perturbation inflow models, used in the present analysis, can be written in a general form as

$$\begin{bmatrix} C_1\lambda_0 & 0 \\ 0 & C_1\lambda_0 \end{bmatrix} \begin{Bmatrix} \lambda_{1c} \\ \lambda_{1s} \end{Bmatrix} = \begin{Bmatrix} -C_{My} \\ C_{Mx} \end{Bmatrix}_{P.A} \tag{17}$$

when $C_1 = 0.5$. Eq. (17) corresponds to Eq. (11) and when $C_1 = 1.0$ it corresponds to Eq. (13).

The concept of equivalent Lock number in the coupled rotor/fuselage type problems appears to involve a certain inconsistency. The fuselage equations of motion in pitch and roll contain terms due to both aerodynamic hub moments and aerodynamic hub forces. When using the perturbation inflow, one can make the observation that only the Lock number associated with the aerodynamic moment terms is modified, however the Lock number associated

with the aerodynamic force terms remains unchanged. Of course, the reason for this inconsistency lies in the formulation of the equations for the inflow variables which are related only to the hub moments, as given in Eq. (4).

Dynamic Inflow Models

The perturbation inflow model does not account for the time lag between the aerodynamic load and the time variation in inflow. The dynamic inflow models represent an extension of the perturbation inflow model by taking into account the time lag between the aerodynamic loading and the response. When using the dynamic inflow model the equations for λ_{1c} and λ_{1s} can be written as

$$\begin{bmatrix} M_1 & 0 \\ 0 & M_1 \end{bmatrix} \begin{Bmatrix} \dot{\lambda}_{1c} \\ \dot{\lambda}_{1s} \end{Bmatrix} + \begin{bmatrix} C_1\lambda_0 & 0 \\ 0 & C_1\lambda_0 \end{bmatrix} \begin{Bmatrix} \lambda_{1c} \\ \lambda_{1s} \end{Bmatrix} = \begin{Bmatrix} -C_{My} \\ C_{Mx} \end{Bmatrix} P.A \tag{18}$$

where M_1 represents the nondimensional apparent inertia associated with the inflow and the quantity C_1 is either 0.5 or 1.0, depending on the definition of mass flow rate. The value of M_1 can be obtained either theoretically or experimentally. Tuckerman[12] evaluated the apparent inertia associated with an impermeable disk subject to an angular acceleration. The nondimensional value of the apparent inertia was found[12] to be $M_1 = 0.1132$. This theoretical value is also supported by parameter identification studies[10]. In Ref. 13, it was noted that M_1 can also be influenced by the pressure distribution on the rotor and hence M_1 could be also assumed to be a function of rotor loading distribution. In Ref. 14, the identified value of M_1 is found to vary between 0.05 to 0.2. In the present analysis, the value of M_1 is assumed to be the theoretically evaluated value i.e., $M_1 = 0.1132$. The implication of using Eq. (18) in rotor dynamic problems[15], under harmonic loadings, can be shown to be equivalent to a modification of the Lock number, which can be written as

$$\gamma^* = \gamma \left[1 - \frac{1}{1 + \frac{16C_1\lambda_0}{\bar{\sigma}a} + \frac{16M_1(i\omega)}{\bar{\sigma}a}} \right] \tag{19}$$

$$= \gamma C$$

Equation (19) indicates that addition of an apparent inertia term to the perturbation inflow model introduces a phase lag between the aerodynamic loads and the response. Furthermore the value of C is now different from the previous values given in Eq. (15) and (16).

The five aerodynamic models, described briefly above, were selected for incorporation in this study. Using these theories, the sensitivity of the aeromechanical stability problem to changes in the aerodynamic assumptions was investigated. For convenience, these five aerodynamic models are concisely summarized below:

Case (a): quasi-steady aerodynamics

Case (b): perturbation inflow model with $C_1=0.5$

Case (c): dynamic inflow model with $C_1=0.5$ and $M_1=0.1132$ which corresponds to Johnson's model[2]

Case (d): perturbation inflow model with $C_1=1.0$

Case (e): dynamic inflow model with $C_1=1.0$ and $M_1=0.1132$

These aerodynamic models can also be viewed as a special case of a general dynamic inflow model. When $M_1=0$, the general inflow model becomes a perturbation inflow model and when $M_1 \to \infty$, the effects of inflow perturbations are totally eliminated and the resulting model is a quasi-steady aerodynamic model.

3. A Brief Summary of the Experiment

A clear description of the experimental set up, used for simulating the fundamental aspects of the aeromechanical stability of a hingeless rotor helicopter, was presented in Ref. 1. The rotor consisted of three blades and five different configurations were tested. The different configurations represent different blade parameters characterized by the nonrotating natural frequencies of the blade in flap and lag, pitch-lag coupling and flap-lag coupling. The rotor was designed such that most of the blade flexibility is concentrated at the root by building in root flexures. The rotor assembly was supported on a gimbal which had pitch and roll degrees of freedom. In this paper the analytical results obtained are compared with the experimental results, presented by Bousman, for rotor configurations 1 and 4, where the designation of these configurations is consistent with those in Bousman's paper[1]. A brief description of these configurations is presented for the sake of completeness, additional information can be found in Refs. 1, 2 and 7. Configuration 1 had different stiffnesses in flap and lag respectively; the corresponding nonrotating flap frequency was 3.13 Hz and that for lead-lag was 6.70 Hz. Configuration 4 was a matched stiffness case where the nonrotating flap frequency was 6.63 Hz and that for lead-lag was 6.73 Hz. The pitch-flap and pitch-lag coupling for these two configurations was zero. For cases where the pitch angle was nonzero, the experimental rotor was designed such that pitch changes were introduced outboard of the flexures and therefore the structural flap-lag coupling for these cases was zero. The blade was also designed to be very stiff in torsion.

4. Method of Solution

The degrees of freedom considered in this aeromechanical stability analysis are: the fundamental flap and lag modes of the blade and the pitch and roll degrees of freedom of the body. In this class of problems, it has been established that the collective flap and lag modes do not couple with the body motion and thus, these modes are not considered. Since the inflow variable λ_1 also has the role of a collective mode, it need not be considered. Therefore, the total number of degrees of freedom governing the aeromechanical problem are six. They are: cyclic flap (β_{1c},β_{1s}), cyclic lead-lag (ζ_{1c},ζ_{1s}), body pitch (θ) and body roll (ϕ). For the cases when the dynamic inflow models are used, two additional degrees of freedom, namely λ_{1c} and λ_{1s}, are also present in the problem.

The solution of the coupled rotor/fuselage problem follows essentially the procedure outlined in Refs. 6 and 7. The procedure for obtaining the stability boundaries of the system consists of the following steps.

1. Evaluation of the equilibrium position of the blade.
2. Linearization of the nonlinear equations of motion about the equilibrium position.
3. Transformation of the linearized equations with periodic coefficients to equations with constant coefficients by using a multiblade coordinate transformation.
4. Evaluation of the eigenvalues of the linearized system with constant coefficients to obtain the stability boundaries.

The eigenvalues appear in complex conjugate pairs, $s = \sigma \pm i\omega$. The real part of the eigenvalue represents the modal damping and the imaginary part modal frequency, respectively. The mode is stable if σ is negative and it is unstable if σ is positive.

In the present problem, the number of complex eigenvalue pairs depends on the type of aerodynamic model used in the analysis. When quasi-steady aerodynamics or the perturbation inflow models are used, there are only six pairs of complex eigenvalues, each one representing one of the six degrees of freedom, namely, β_{1c}, β_{1s}, ζ_{1c}, ζ_{1s}, θ and ϕ. The modes corresponding to the rotor degrees of freedom (β_{1c}, β_{1s}, ζ_{1c}, ζ_{1s}) are referred to either progressing or regressing mode depending on the numerical value of the rotating natural frequency. A more detailed description of this terminology can be found in Refs. 3 and 7. When the dynamic inflow model is used, the six eigenvalue pairs are augumented by one additional pair of eigenvalues corresponding to the inflow variables. Since the equations for the inflow variables λ_{1c} and λ_{1s} are given in first order state variable form, Eq. (18) the stability analysis will yield only one pair of eigenvalue corresponding to these two inflow variables. The mode corresponding to this eigenvalue pair is designated as the "inflow mode", (λ), following Johnson's[2] terminology.

5. Results and Discussion

In the present study, aimed at predicting the aeromechanical stability of a model helicopter, the behavior of the model is studied at various values of rotor speed Ω. Two rotor configurations are analyzed. Configuration 1, in which the nonrotating flap frequency is lower than the nonrotating lag frequency, and configuration 4, in which these two frequencies are almost equal, which corresponds to a matched stiffness configuration. These different configurations have an influence on the dynamic behavior of the coupled rotor/fuselage system. In a matched stiffness configuration the structural flap-lag coupling is eliminated. Furthermore the root torsional moment due to the combined flap-lag motion, which is somewhat similar to an effective flap-pitch and lag-pitch coupling, is also eliminated. It should be mentioned however that these effective flap-pitch and lag-pitch couplings are not structural couplings. It was mentioned in the previous section that the experimental model was designed so as to eliminate structural flap-lag coupling, for these configurations. Therefore, the difference between these two configurations consists of the root torsional moment due to combined flap-lag motion which is present in configuration 1 and absent in configuration 4. This root moment acts as an exciting moment for the body pitch and roll motions.

The numerical data used in the analysis is presented in the Appendix. It should be mentioned that the roll inertia used in the present calculations is slightly higher than the value (183 gm$\cdot$m^2) provided in Ref. 1. The value for roll inertia used in our calculation is 194 gm$\cdot$m^2 which is 6% higher than 183 gm$\cdot$m^2. This value of roll inertia was obtained by using the body spring stiffness in roll, provided by Bousman[16], such that the calculated nonrotating coupled roll frequency matches the measured frequency.

5.1 Results for Configuration 1

The results for Configuration 1 are presented in Figs. 1-8. The variation of various modal frequencies with Ω are shown in Figs. 1-2, together with the experimental data, taken from Ref. 1. It can be seen from Fig. 1 that the analysis with quasi-steady aerodynamics predicts the modal frequencies which are in excellent agreement with the experimental results. Figure 2 presents the calculated modal frequencies for Case (b), perturbation inflow with C_1=0.5, and Case (c) dynamic inflow model with C_1=0.5 and M_1=0.1132. With the perturbation inflow model, the predicted frequencies for roll (ϕ) and pitch (θ) are over estimated in the range Ω > 300 R.P.M.. On the otherhand, by incorporating a time delay in the inflow model, Case (c), the calculated pitch and roll frequencies are in good agreement with the measured values. However, the predicted pitch frequency is still slightly higher in the range Ω > 300 R.P.M. A similar trend was also observed in the results for Case (d), perturbation inflow model, with C_1=1.0, and Case (e) dynamic inflow model with C_1=1.0 and M_1=0.1132.

It was mentioned earlier that the analysis with dynamic inflow model produces an additional eigenvalue corresponding to the inflow mode (λ). For Case (c), there are two eigenvalues with frequencies below 0.6 Hz in the range Ω > 200 R.P.M. as evident from Fig. 2. The frequency corresponding to one mode remains almost constant ($\simeq$0.5 Hz), while the other decreases to zero and then increases. It is difficult to identify which one of these two corresponds to the flap regressing mode (β_R) and which one should be associated with the inflow mode (λ). The mode with the constant frequency, in Fig. 2, is identified as inflow mode (λ) and the other mode is identified as flap regressing mode (β_R). Johnson[2] also identified the mode with a constant frequency as inflow mode (λ) and the second mode as flap regressing mode (β_R). Some additional comments on this identification procedure will be made later.

Figure 3 presents the variation of damping in flap regressing mode (β_R) and inflow mode (λ) with Ω. It is evident from Fig. 3 that the damping in the flap regressing mode increases rapidly with Ω for the analysis with quasi-steady aerodynamics. The introduction of the perturbation inflow model with C_1=0.5, Case (b), drastically reduces the damping in β_R mode. This reduction in damping is caused by reduced aerodynamic damping with perturbation inflow. For this case the relevant quantities are: solidity ratio σ = 0.0494; lift curve slope a = 5.73 and steady inflow λ_0=0.014.

Therefore the deficiency function C, based on Eq. (15), is C=C.284. Hence, the effective Lock number $\gamma^*=0.284\gamma$. This shows that perturbation inflow reduces the magnitude of aerodynamic forces by approximately 72%. In the case of dynamic inflow with $C_1=0.5$ and $M_1=0.1132$, Case (c), the damping in the mode which is identified as the inflow mode (λ) remains relatively low, but the damping in flap regressing mode (β_R) increases with Ω. These results indicate that the damping in flap regressing mode reverts to the value obtained in the analysis with quasi-steady aerodynamics, as a consequence of the time delay present in dynamic inflow model. This seems to contradict the earlier results published in Refs. 9, 10 and 17. It was mentioned in Ref. 17 that flap regressing mode damping is substantially decreased by dynamic inflow for small values of collective pitch setting of the blade. Furthermore, it was found in Ref. 10 that dynamic inflow reduces the damping in flap regressing mode. This raises a question whether the inflow mode identified in Fig. 2, and also identified as such by Johnson[2], is a flap regressing mode and the mode identified as the flap regressing mode is really an inflow mode. To ascertain the reliability of this identification procedure, the eigenvectors corresponding to these modes were also analyzed. Table I shows the eigenvectors corresponding to the mode identified as the flap regressing (β_R) and the inflow mode (λ) at Ω = 900 R.P.M. It can be seen that in the flap regressing mode, the flap motion has a higher participation factor than the inflow variables. In the inflow mode, the flap and inflow variables have almost equal participation factor. Also in this (λ) mode, the pitch and roll motions have substantial participation factors. However, from these results, one can conclude that the flap regressing mode and inflow mode are highly coupled modes.

Figures 4 and 5 illustrate the variations of damping in pitch as a function of Ω. Using quasi-steady aerodynamics, a higher damping, in the range $200 < \Omega < 800$ R.P.M. is predicted as evident from Fig. 4. However when dynamic inflow, Case (c), with $C_1=0.5$ and $M_1=0.1132$ is used the damping is predicted very well in the range $200 < \Omega < 800$ R.P.M., however the damping is somewhat under predicted beyond Ω = 800 R.P.M. Figure 5 shows that using the dynamic inflow model, Case (e) with $C_1=1.0$ and $M_1=0.1132$, the damping predictions are in very good agreement with the experimental results over the complete range of Ω. When the value of C_1 is increased from 0.5 to 1.0, in the dynamic inflow models, one finds that the corresponding damping in pitch increases by 10% ~ 25% for $\Omega > 400$ R.P.M. It is also evident from Figs. 4-5 that perturbation inflow models do not seem to predict the correct damping levels.

The variation of damping in roll mode is shown in Figs. 6-7. When using quasi-steady aerodynamics, the damping, in the range of $\Omega > 500$ R.P.M., is over predicted as evident from Fig. 6. Using the perturbation inflow model, with $C_1=0.5$, Case (b), the damping in the range of $\Omega < 600$ R.P.M. is under estimated, beyond this range of Ω, the predictions are good. The damping levels predicted using the dynamic inflow model, with $C_1=0.5$ and $M_1=0.1132$, Case (c), are in good agreement with experimental data over the whole range of Ω, as shown in Fig. 6. It can be seen from Fig. 7 that calculations with the perturbation inflow model, with $C_1=1.0$, Case (d), yield damping levels which are too low in the range $\Omega < 500$ R.P.M. and too high for the range $\Omega > 600$ R.P.M. Calculations with the dynamic inflow model, with $C_1=1.0$ and $M_1=0.1132$, Case (e), also overpredict the damping in the range $\Omega > 700$ R.P.M. It should be mentioned, that in the range $\Omega > 700$ R.P.M., when using dynamic inflow models, the percentage increase in roll damping as a result of increasing C_1 from 0.5 to 1.0 is 5% to 12%.

Based on the results obtained for the damping in the pitch and roll modes, it appears that the theoretical results are quite sensitive to the value selected for C_1. It is also evident that introduction of a time delay in the inflow model seems to be an important factor. Based on the overall agreement with the experimental data, it appears that the dynamic inflow model with $C_1=0.5$ and $M_1=0.1132$, Case (c), seems to be somewhat superior to the dynamic inflow model with $C_1=1.0$ and $M_1=0.1132$, Case (e).

Figure 8 presents the variation of regressing lag mode damping with Ω. The predicted damping levels are in good agreement with the experimental results in the range $\Omega < 700$ R.P.M. and $\Omega > 900$ R.P.M. for all the aerodynamic models used. For the cases analyzed with perturbation inflow models, Case (b) with $C_1=0.5$ and Case (d) with $C_1=1.0$, the value of Ω at which the resonant peak occurs is shifted from 760 R.P.M. to 800 R.P.M. This shift is associated with the fact that when using both models the roll frequency predicted is higher than the experimental result and as a consequence, the resonance is also shifted to a higher value of Ω. Calculations with quasi-steady aerodynamics predict correctly the value of Ω at which resonance occurs, however the stability of this mode is overpredicted. In the analyzes with dynamic inflow models, the predicted damping levels are in excellent agreement with the experimental results, including the damping at resonance. The level of agreement with experimental data found in this case is somewhat better than those shown in Refs. 1 and 2. This result seems to support the statement made in Ref. 7, that the coupled rotor/fuselage model derived in Ref. 5 is a reasonably accurate model for the configuration tested in Ref. 1.

5.2 Results for Configuration 4

The results for Configuration 4 are presented in Figs. 9-16. Figures 9 and 10 show the variation of modal frequencies as a function of Ω. It can be seen from Fig. 9 that all the frequencies except the one corresponding to 0.7 Hz are predicted well by the quasi-steady aerodynamic model. In the range $250 < \Omega < 350$ R.P.M., the pitch, roll and flap regressing modes undergo a change in their characteristics. The flap regressing mode (β_R) becomes a roll mode (ϕ) and roll mode (ϕ) becomes a pitch mode (θ) and the pitch mode (θ) becomes a flap regressing mode (β_R). In this range of Ω, the predicted roll frequencies are higher than the measured values. Quasi-steady aerodynamics is incapable of predicting a frequency close to 0.7 Hz in the range $300 < \Omega < 1000$ R.P.M. Figure 10 illustrates the results for the cases where the perturbation inflow model, Case (b) with $C_1=0.5$ and dynamic inflow model, Case (c), with $C_1=0.5$ and $M_1=0.1132$, were used. Although calculations based on the perturbation inflow model are capable of predicting a frequency close to the experimentally measured frequency of 0.7 Hz, the pitch and roll modes frequencies are overpredicted. With dynamic inflow

model, all the frequencies are predicted well. However, in the range $250 < \Omega < 350$ R.P.M., the roll mode frequency is still overpredicted. In this range of Ω, none of the aerodynamic models used in the present study, is capable of correctly predicting the roll frequency. Johnson[18] attributed this discrepancy to either the deficiency of the aerodynamic model or the presence of some higher mode of the rotor or body. In any case, this problem remains unresolved. In the range $\Omega > 400$ R.P.M., the mode with a frequency close to 0.7 Hz is identified as inflow mode (λ) and the other mode with a frequency which is lower than 0.7 Hz is identified as flap regressing mode (β_R). This identification is based on the analysis of the eigenvectors corresponding to these two modes. Table II shows the eigenvectors of the identified inflow mode and flap regressing mode, for $\Omega = 900$ R.P.M. In this case, as in Configuration 1, these two modes are highly coupled. However, in the β_R mode, the flap motion has a higher participation factor than the participation of the inflow variables. In the λ mode, the body pitch has the highest participation factor, with the flap, body roll and inflow having almost equal participation factors. As a result of this identification procedure one finds that using the dynamic inflow model the damping for the flap regressing mode is predicted to have a value comparable to that obtained when using quasi-steady aerodynamics. This seems to contradict some results which have been published earlier in Refs. 9, 10 and 17 where it was found that using dynamic inflow yields a substantial reduction in regressing flap mode damping.

The variation of roll damping as a function of Ω is illustrated in Figs. 11-12. Calculations based on quasi-steady aerodynamics overpredict the damping in the range $\Omega > 300$ R.PM., as evident in Fig. 11. Calculations based on the perturbation inflow model, with $C_1=0.5$, under predicts the damping in the range $\Omega < 800$ R.P.M. The damping levels predicted by using the dynamic inflow model, with $C_1=0.5$ and $M_1=0.1132$, are in reasonable agreement with the experimental values. From Fig. 12, it is evident that using the perturbation inflow model with $C_1=1.0$, yields a damping prediction which is too high for $\Omega > 700$ R.P.M. Using the dynamic inflow model, with $C_1=1.0$ and $M_1=0.1132$, yields damping level predictions which are in reasonable agreement with the experimental results.

The variation of damping for the pitch mode (θ) and the mode which has been identified as the inflow mode (λ) are presented in Figs. 13 and 14. It is evident from Fig. 13 that predictions based on quasi-steady aerodynamics yield higher values of damping than the measured values. Calculations based on dynamic inflow, with $C_1=0.5$ and $M_1=0.1132$, predict the pitch damping well, but the damping associated with the inflow mode (λ) is lower than the experimental values. Figure 14 shows that using the dynamic inflow model, with $C_1=1.0$ and $M_1=0.1132$, yields a higher value of pitch damping than measured in the test. The damping in inflow mode is also higher than the experimental values. From the results shown in Figs. 13 and 14, it is evident that an increase in the value of C_1 from 0.5 to 1.0 increases the pitch mode damping by about 25%. Therefore, it can be concluded that for Configuration 4, as well as Configuration 1, the predicted damping levels in pitch and roll modes are quite sensitive to the dynamic inflow model used in the analysis. By using a different combination of the values of C_1 and M_1, better correlation with the experimental results could have been achieved. However, among the aerodynamic models employed in the present study, the dynamic inflow with $C_1=0.5$ and $M_1=0.1132$, Case (c), yields better agreement with the experimental results than the other aerodynamic models.

The variation of lag regressing mode damping with Ω is shown in Fig. 15. The resonant frequency obtained with the perturbation inflow models exhibits a shift to a higher value of Ω than the one observed in the experiment. Calculations based quasi-steady aerodynamics predict the damping levels and the resonant frequency very well, the mode is more stable at resonance, than the stability indicated in the test. Calculations with the dynamic inflow models yield results which are in excellent agreement with the experimental data.

Figure 16 shows the variation of regressing lag mode damping as a function of collective pitch setting of the blade, at $\Omega = 1000$ R.P.M. Calculations with the dynamic inflow model, using $C_1=0.5$ and $M_1=0.1132$, yields damping values which are in very good agreement with the measured values.

6. Conclusions

The aeromechanical stability of a helicopter in ground resonance is analyzed, using five different aerodynamic models and the analytical results are compared with the experimental results. Based on the comparison, the following conclusions can be drawn:

(1) For the aeromechanical stability problem studied here, the perturbation inflow models do not predict correctly the modal frequencies and damping.

(2) Quasi-steady aerodynamics predicts the modal frequencies very well for Configuration 1, but is incapable of predicting a frequency of 0.7 Hz measured in the experiment, for Configuration 4. The damping in body roll and pitch modes are over predicted. The regressing lag mode damping is predicted well.

(3) The dynamic inflow models predict the modal frequencies and damping values which are in very good agreement with the experimental results. This implies that for the present problem the time lag is an important ingredient in the dynamic inflow model.

(4) The predicted damping levels for the lag regressing mode, using dynamic inflow models, are in excellent agreement with the experimental results including the value at resonance. This indicates that the mathematical model for the coupled rotor/fuselage system is accurate.

(5) From the cases studied with dynamic inflow models, it is evident that the predicted damping levels for the body modes, increase when C_1 is increased from 0.5, Case (c), to 1.0, Case (e). For both rotor configurations, the pitch damping increases by 10% to 25% and the roll damping increases by 5% to 12%.

(6) Based on the comparison of results obtained with various aerodynamic models, it seems that the

dynamic inflow model with C_1=0.5 and M_1=0.1132 is the most suitable aerodynamic model, for the specific aeromechanical problem studied in this paper.

(7) Identification of the flap regressing mode and the inflow mode proved itself to be quite complicated. These modes were identified by using the frequency information together with a careful examination of the eigenvectors. The results based on this identification procedure seem to indicate that when using the dynamic inflow model the predicted values of damping for the regressing flap mode are comparable to those obtained with quasi-steady aerodynamics.

References

1. Bousman, W.G., "An Experimental Investigation of the Effects of Aeroelastic Couplings on Aeromechanical Stability of a Hingeless Rotor Helicopter", Journal of the American Helicopter Society, Vol. 26, No. 1, Jan. 1981, pp. 46-54.

2. Johnson, W., "Influence of Unsteady Aerodynamics on Hingeless Rotor Ground Resonance", Journal of Aircraft, Vol. 19, No. 8, Aug. 1982, pp. 668-673.

3. Johnson, W., Helicopter Theory, Princeton University Press, Princeton, New Jersey, 1980.

4. Johnson, W., "A Comprehensive Analytical Model of Rotorcraft Aerodynamics and Dynamics", NASA TM 81182, June 1980.

5. Venkatesan, C. and Friedmann, P.P., "Aeroelastic Effects in Multirotor Vehicles with Application to a Hybrid Heavy Lift System, Part I: Formulation of Equations of Motion", NASA CR 3288, August 1984.

6. Venkatesan, C. and Friedmann, P.P., "Aeroelastic Effects in Multirotor Vehicles, Part II: Method of Solution and Results Illustrating Coupled Rotor/Body Aeromechanical Stability", NASA CR Report, Submitted for publication.

7. Friedmann, P.P., and Venkatesan, C., "Comparison of Experimental Coupled Helicopter Rotor/Body Stability Results with a Simple Analytical Model", Paper Presented at the Integrated Technology Rotor (ITR) Methodology Workshop, NASA Ames Research Center, Moffett Field, California, June 20-21, 1983, to be published in the Journal of Aircraft, November 1984.

8. Greenberg, J.M., "Airfoil in Sinusoidal Motion in a Pulsating Flow", NACA TN 1326, 1947.

9. Peters, D.A. and Gaonkar, G.H., "Theoretical Flap-Lag Damping with Various Dynamic Inflow Models", Journal of the American Helicopter Society, Vol. 25, No. 3, July 1980, pp. 29-36.

10. Banerjee, D., Crews, S.T., Hohenemser, K.H., and Yin, S.K., "Identification of State Variables and Dynamic Inflow from Rotor Model Dynamic Tests", Journal of the American Helicopter Society, Vol. 22, No. 2, April 1977, pp. 28-36.

11. Curtiss, H.C., Jr. and Shupe, N.K., "A Stability and Control Theory for Hingeless Rotors", Annual National Forum of the American Helicopter Society, Washington, D.C., May 1971.

12. Tuckerman, L.B., "Inertia Factor of Ellipsoids for Use in Airship Design", NACA Report No. 210, 1925.

13. Pitt, D.M. and Peters, D.A., "Theoretical Prediction of Dynamic Inflow Derivatives", Vertica, Vol. 5, No. 1, 1981, pp. 21-34.

14. Banerjee, D., Crews, S.T. and Hohenemser, K.H., "Parameter Identification Applied to Analytic Hingeless Rotor Modelling", Journal of the American Helicopter Society, Vol. 24, No. 1, Jan. 1979, pp. 26-32.

15. Peters, D.A., "Hingeless Rotor Frequency Response with Dynamic Inflow", NASA SP-352, Vol. 1, 1974.

16. Bousman, W., Private Communication, Oct. 1983.

17. Ormiston, R.A., "Application of Simplified Inflow Models to Rotorcraft Dynamic Analysis", Journal of the American Helicopter Society, Vol. 21, No. 2, July 1976, pp. 34-37.

18. Johnson, W., "The Influence of Unsteady Aerodynamics on Hingeless Rotor Ground Resonance", NASA TM 81302, July 1981.

Appendix

Rotor Geometry

Number of blades	3
Radius, cm	81.1
Chord, cm	4.19
Hinge offset, cm	8.51
Blade Airfoil	NACA 23012
Profile drag coefficient	0.0079
Lock number	7.37
Solidity ratio	0.0494
Lift curve slope	5.73
Height of rotor hub above gimbal, cm	24.1

Blade Mass Properties

Blade mass (to flap flexures), gm	209
Blade mass centroid (Ref. flexure centerline), cm	18.6
Blade flap inertia (Ref. flexure centerline), $gm \cdot m^2$	17.3

Blade Frequency and Damping

	Conf. 1	Conf. 4
Nonrotating Flap frequency, Hz	3.13	6.63
Nonrotating Lag frequency, Hz	6.70	6.73
Damping in lead-lag (% critical)	0.52%	0.53%

Body Mass Properties

Rotary inertia in pitch, $gm \cdot m^2$	633
Rotary inertia in roll, $gm \cdot m^2$	194

Body Stiffness and Damping

Pitch stiffness, $gm \cdot cm^2/sec^2 \cdot rad$	0.8687×10^9
Roll stiffness, $gm \cdot cm^2/sec^2 \cdot rad$	0.1113×10^{10}
Damping in roll (% critical)	0.929%
Damping in pitch (% critical)	3.20%
Pitch frequency, Hz	1.86
Roll frequency, Hz	3.81

Table I. Eigenvectors of Flap Regressing (β_R) and Inflow (λ) modes at Ω = 900 R.P.M. for Configuration 1

Degree of freedom	Flap Regressing mode β_R	Inflow mode λ
β_{1C}	1.000	.989
β_{1S}	.593	1.000
ζ_{1C}	.012	.020
ζ_{1S}	.030	.020
ϕ	.072	.563
θ	.034	.718
λ_{1C}	.475	.779
λ_{1S}	.377	.765

Table II. Eigenvectors of Flap Regressing (β_R) and Inflow (λ) modes at Ω = 900 R.P.M for Configuration 4

Degree of freedom	Flap Regressing mode β_R	Inflow mode λ
β_{1C}	.584	.763
β_{1S}	1.000	.785
ζ_{1C}	.033	.013
ζ_{1S}	.023	.013
ϕ	.166	.745
θ	.050	1.000
λ_{1C}	.426	.619
λ_{1S}	.545	.592

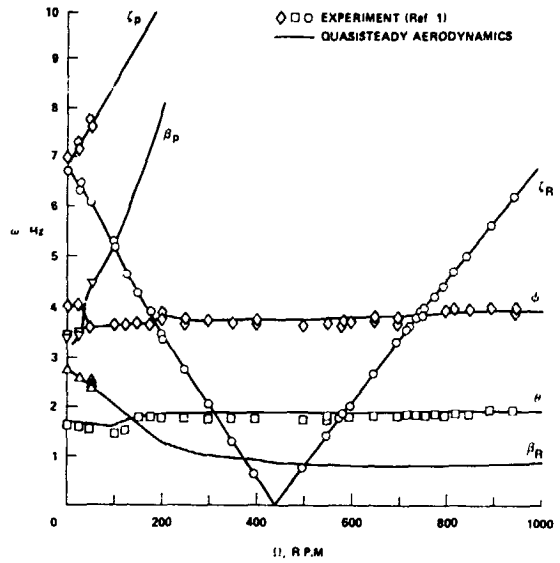

Fig. 1 Modal Frequencies as a Function of Ω; θ_c=0; Configuration 1

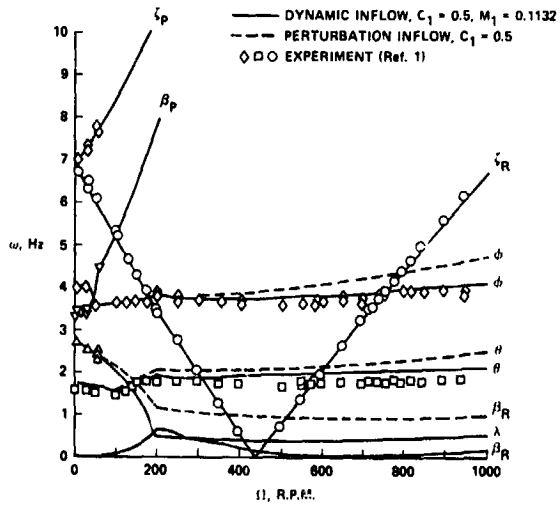

Fig. 2 Modal Frequencies as a Function of Ω; θ_c=0; Configuration 1

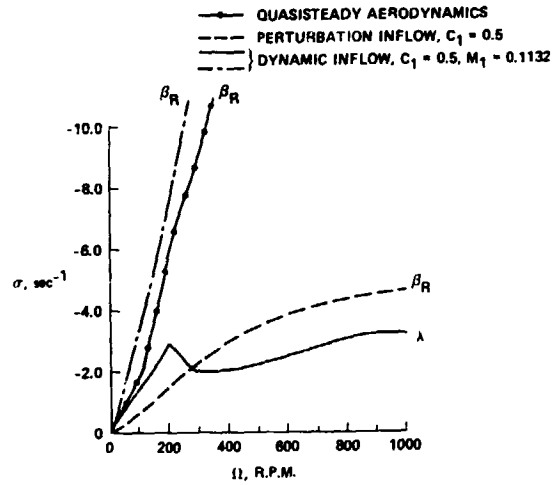

Fig. 3 Variation of Damping in Regressing Flap Mode and Inflow Mode with Ω; θ_c=0; Configuration 1

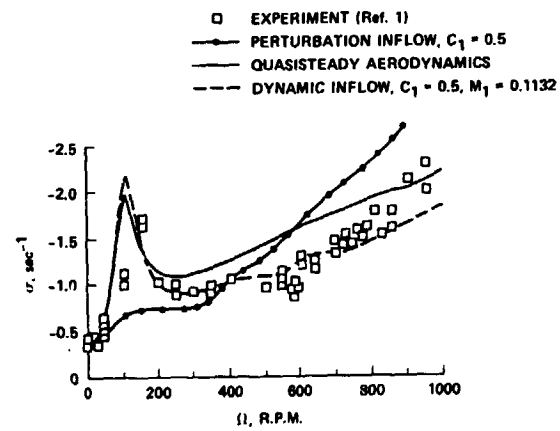

Fig. 4 Body Pitch Mode Damping as a Function of Ω; θ_c=0; Configuration 1

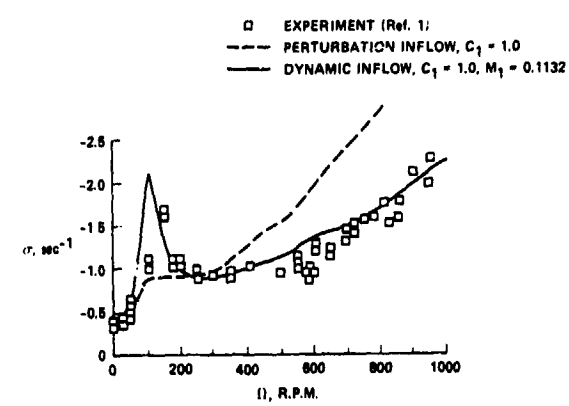

Fig. 5 Body Pitch Mode Damping as a Function of Ω; θ_c=0; Configuration 1

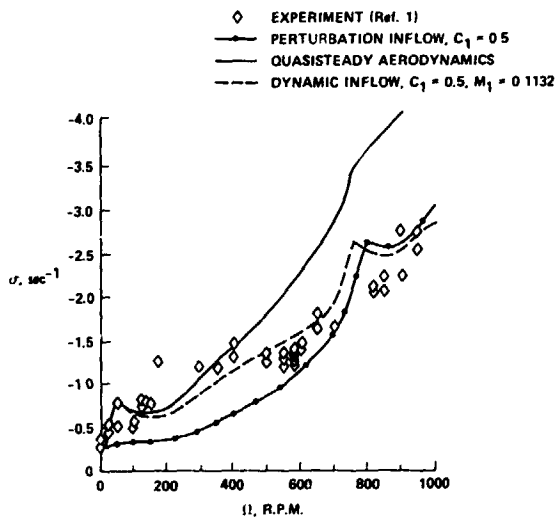

Fig. 6 Body Roll Mode Damping as a Function of Ω; θ_c=0; Configuration 1

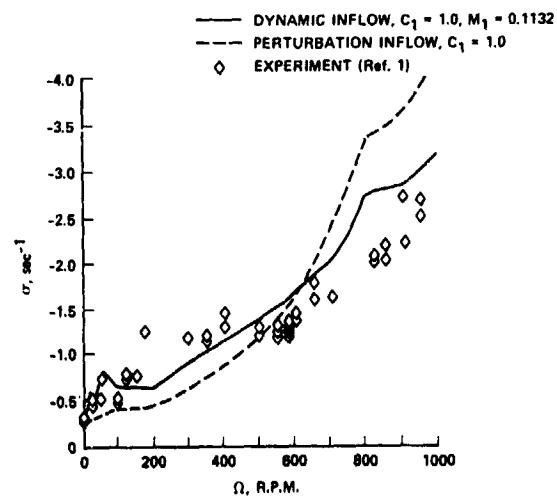

Fig. 7 Body Roll Mode Damping as a Function of Ω; θ_c=0; Configuration 1

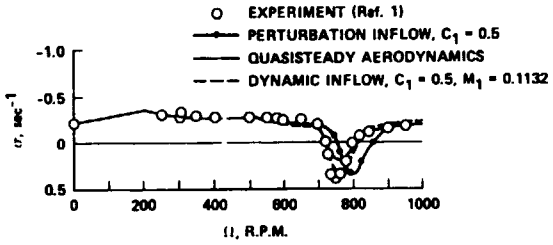

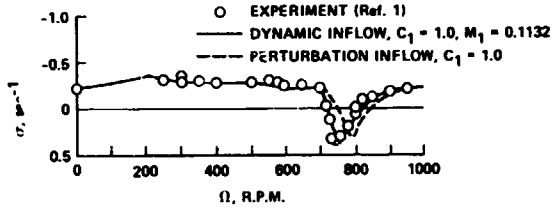

Fig. 8 Regressing Lag Mode Damping as a Function of Ω; θ_c=0; Configuration 1

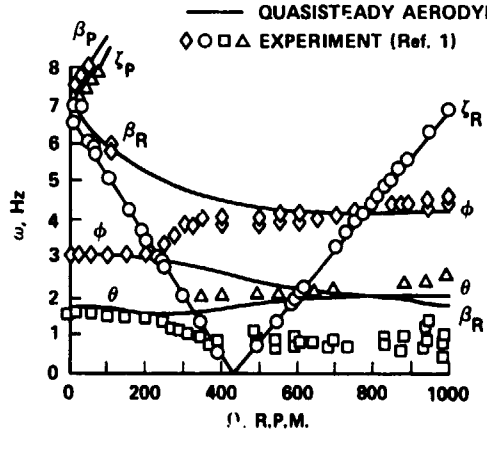

Fig. 9 Variation of Modal Frequencies with Ω; θ_c=0; Configuration 4

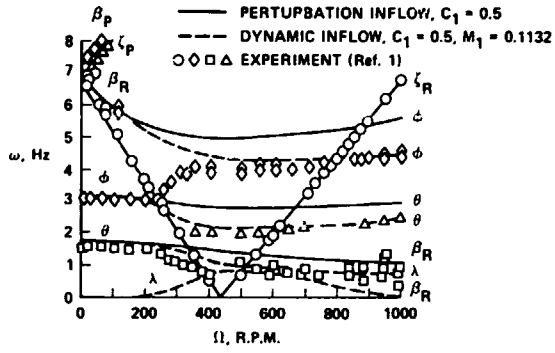

Fig. 10 Variation of Modal Frequencies with Ω; θ_c=0; Configuration 4

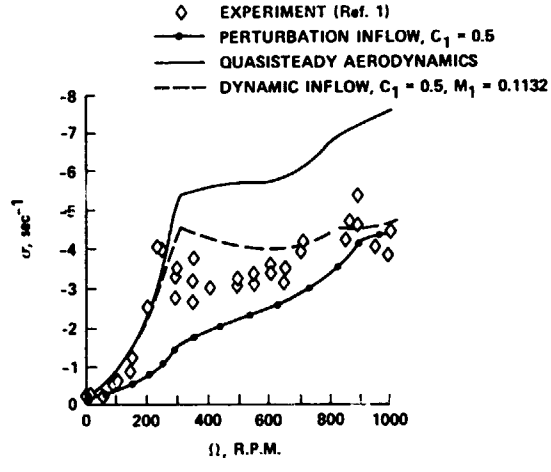

Fig. 11 Variation of Roll Mode Damping with Ω; θ_c=0; Configuration 4

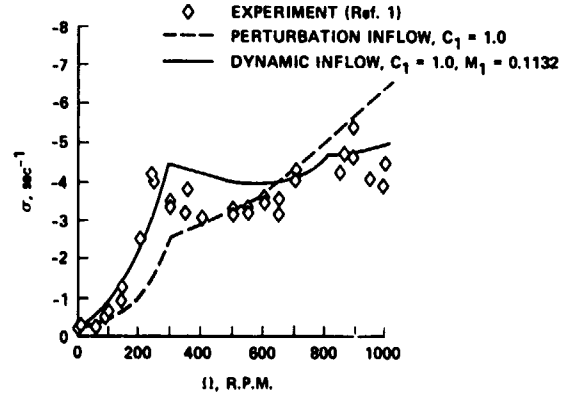

Fig. 12 Variation of Roll Mode Damping with Ω; θ_c=0; Configuration 4

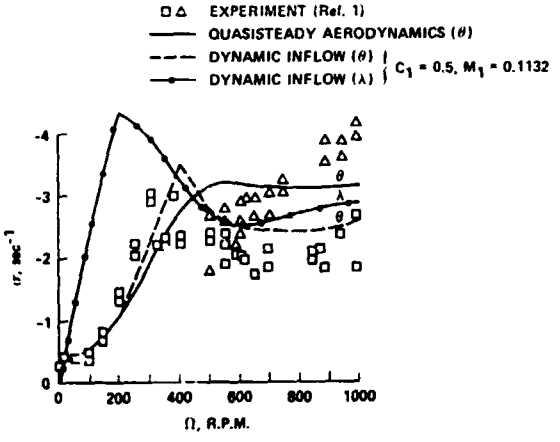

Fig. 13 Variation of Pitch (θ) and Inflow (λ) Modes Damping with Ω; θ_c=0; Configuration 4

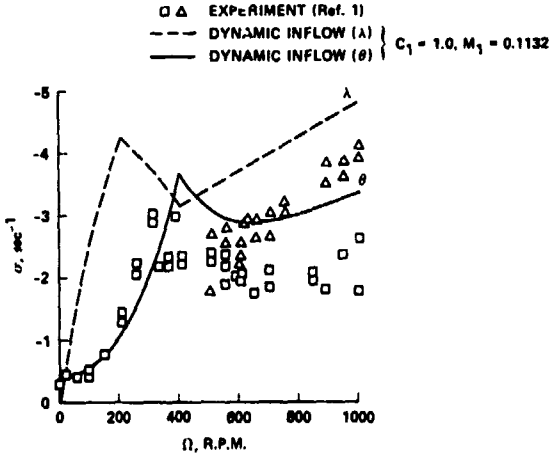

Fig. 14 Variation of Pitch (θ) and Inflow (λ) Modes Damping with Ω; θ_c=0; Configuration 4

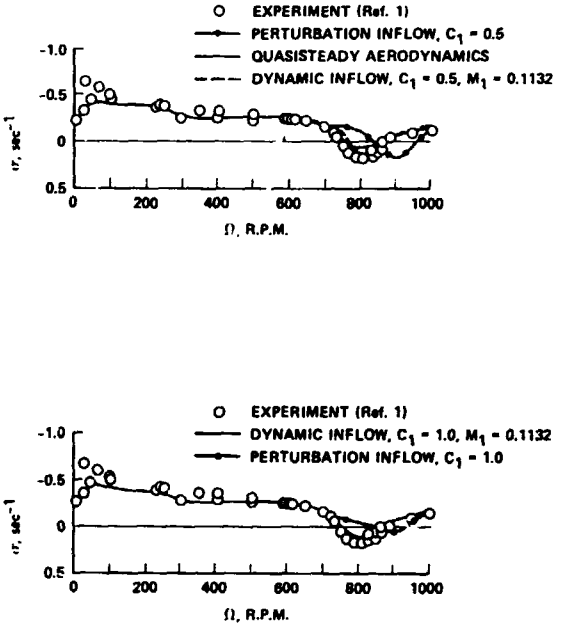

Fig. 15 Regressing Lag Mode Damping as a Function of Ω; θ_c=0; Configuration 4

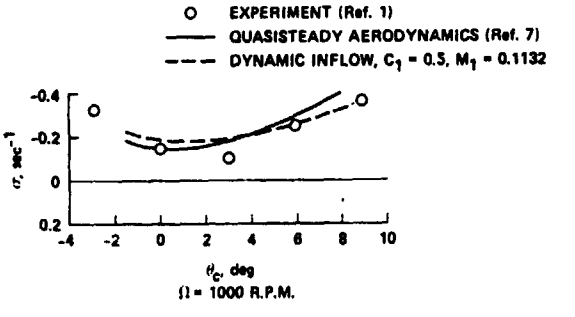

Fig. 16 Regressing Lag Mode Damping as a Function of θ_c; Configuration 4

DISCUSSION
Paper No. 14

INFLUENCE OF VARIOUS UNSTEADY AERODYNAMIC MODELS ON THE AEROMECHANICAL STABILITY OF A HELICOPTER IN GROUND RESONANCE
P. P. Friedmann
and
C. Venkatesan

Bill Bousman, U.S. Army Aeromechanics Laboratory: Jack Landgrebe put a perspective on dynamic inflow as not really contributing to the loads problem and I think that the conclusions from the first two papers show that although it has a strong effect on the flapping degree of freedom, from the designer's point of view, it is not really important for the lag degree of freedom. I guess my question is to all three of these guys. Are there applications for dynamic inflow in something like the handling qualities area where simulation needs the speed of the model and has any work been done in here or are there paths that we should be going?

Friedmann: I'll tell you I was expecting this question so I have a slide. "Can I have the slide, please?" The last slide [Fig. 3] is something which in your experiment you might have data, but it wasn't in your paper so I don't know whether you have data or not. It shows the flap regressing mode damping with various kinds of aerodynamics. What it really shows you is that the damping with quasisteady aerodynamics is here. If you put in the perturbation inflow it knocks down this damping in the flap mode very significantly. And when you put in the dynamic inflow with C_1 of 0.5 it brings it up again to almost where the damping was with the quasisteady aerodynamics. You can also see how the damping of inflow mode changes as a function of Ω. So in relation to the first question which you have asked I think that the better test for how much global truth is in dynamic inflow should really be based on the behavior of the flapping mode as has been indicated by both Dave Peters and [Gopal] Gaonkar. Maybe in the future some calculations associated with that type of examination could be revealing.

Dave Peters, Washington University: On the question about handling qualities, I think it definitely has an effect. There was one figure in the paper we didn't show which shows the pitch and roll moment on the rotor due to a roll oscillation or a pitch oscillation. As you go to an ω of zero the slope of that curve then is the roll rate or pitch rate moment as a function of θ_s or θ_c, like a control derivative. There's more than a factor of two difference with or without dynamic inflow; almost a factor of three in one case. I think if you are going to do handling qualities, anything in the less than once per frequency range then the dynamic inflow is going to have importance. That's a great paper, Peretz. I think we should have an altar call and everyone who wants to put dynamic inflow in their analysis should come forward or something after a paper like that because it's really good. One question I had--on a model like yours, how much extra complexity does it take to put the dynamic inflow in? Is it 2% or 10%? Maybe you can give us a feeling for that.

Friedmann: It may be 10% additional work. It's not really very difficult to do. Particularly if you have somebody as good as Venkatesan who does it.

Bob Loewy, Rensselaer Polytechnic Institute: My question pertains to the off-diagonal terms in the L matrix and really takes up a little bit on Euan Hooper's earlier question on the earlier paper. And that is it seems to me that swirl would make those kind of terms nonzero and that particularly in tilt rotors and high speed forward flight you would expect more swirl than we are used to. I wonder if you have thought about these things?

Friedmann: I have to phrase this very carefully. I am essentially somebody who uses dynamic inflow. I am not a person who has ambitions of improving dynamic inflow. I am a believer in unsteady aerodynamics and as a consequence you might be aware a year ago one of my students completed an arbitrary motion type of unsteady airfoil theory in which you can essentially do the same things you do with dynamic inflow, but for hover and forward flight. It is based on essentially an assumed wake. [It has] all the mathematical complexities and maybe mathematical fundamentals which an unsteady aerodynamics theory provides you and you don't have to use the assumptions which are embedded in dynamic inflow and cannot be removed. We have used this particular arbitrary motion theory to essentially extend the so-called Loewy lift deficiency function, which you might be familiar with, to arbitrary motions. In that AIAA paper which was given last year we have not been very successful. But since then Dr. Venkatesan has managed to do an arbitrary motion approximation to the theory and that theory can probably be used to capture the same behavior which is predicted by the dynamic inflow model and you might be able to see whether based on such a theory you do get off-diagonal terms or not.